OPEN

NPG Asia Materials (2013) 5, e49; doi:10.1038/am.2013.17

www.nature.com/am

ORIGINAL ARTICLE

Surface plasmon-enhanced gas sensing in single gold-peapodded silica nanowires

Sheng-Bo Wang[1], Yi-Fan Huang[2,3], Surojit Chattopadhyay[3,4], Shoou Jinn Chang[1], Ruei-San Chen[5], Cheong-Wei Chong[6], Ming-Shien Hu[2], Li-Chyong Chen[6] and Kuei-Hsien Chen[2,6]

An intriguing system featuring a wide band gap silica nanowire (SiO_x NW) that absorbs visible light (532 nm) via the surface plasmons (SPs) of embedded gold nanoparticles (Au NPs) is reported for sensing applications. We report SP resonance-enhanced molecular oxygen sensing by single Au-NPs@SiO_x NWs under 532-nm illumination (visible light) at room temperature. Excellent selectivity of the Au-NPs@SiO_x NWs to molecular oxygen in air has been demonstrated. Illumination improved the sensing properties in terms of response and fast recovery time, which can be attributed to the photogenerated hole-mediated oxygen desorption. A general strategy of light-modulated sensing, vis-à-vis dark, is demonstrated in a wide band gap single NW system that could potentially open up routes for biosensing, because silica and Au both lack biotoxicity.
NPG Asia Materials (2013) **5,** e49; doi:10.1038/am.2013.17; published online 24 May 2013

Keywords: gas sensor; nanowire; silica; surface plasmon

INTRODUCTION

Oxide-based semiconductor nanostructured materials have been widely investigated for chemical and biosensing applications because of their biocompatibility, relatively easy large-scale synthesis, superior thermal and chemical stabilities and high surface-to-volume ratios.[1,2] However, improving the sensing performance requires improved sensitivity, good selectivity or specificity, short rise and fall times of signals (high-speed response and recovery) and an easily attainable working temperature, ideally in the room-temperature range. Because of their large surface areas, nanostructures such as nanowires (NWs),[3] nanotubes,[4,5] nanorods[6] and nanoparticles (NPs)[7] offer large reaction cross sections for signal generation. To further enhance the sensing performance of these nanostructures, surface modification,[8–10] applications of high electrical bias[11] and high operational temperatures ($T > 100\,^{\circ}C$)[12] have been used.

Improving the sensing performance with light has also been demonstrated using ZnO-based nanostructures under UV illumination.[13] However, most of these approaches have required high operational temperatures, high biases and light outside the visible range (400–800 nm), which has somewhat limited their general applicability. We demonstrated how Au NPs embedded in single amorphous silica NW (Au-NPs@SiO_x silica NW) can be used as an oxygen gas sensor by amperometric routes in this work. According to that study, the silica shell is amorphous, containing various defects within the NW, such as nonbridging oxygen atoms, dangling bonds, strain bonds and oxygen vacancies, and the silica matrix is nonstoichiometric (SiO_x instead of SiO_2).[14] These Au-NPs@silica NW properties make them sensitive to oxygen molecules, which changes the conductance of the single-NW system to enable sensing. We subsequently reported the interesting plasmonic behavior of the Au-NPs@silica NW system that also changes its electrical properties.[14,15] Although silica NWs are nonconducting, photoconductance is observed via the surface plasmon resonance (SPR) absorption of visible light at ~532 nm. Hsieh *et al.*[16] have also reported similar results in a system of Au NPs encapsulated in monoclinic Ga_2O_3 NWs. The SP intensity distribution was studied and elucidated using the scanning transmission electron microscope (TEM)—electron energy-loss spectroscopy technique.[17] The results reveal an anisotropic SP field distribution of the Au NPs with higher intensities in the radial (transverse mode) than in the axial (longitudinal mode) direction of the NW. The photocurrent of Au-NPs@silica NWs shows an enhancement of ~15% when the incident polarization is transverse over that of longitudinal polarization. This enhanced photocurrent suggests that photogenerated carriers affect the surface-carrier concentration and would be critical in gas sensing, because adsorption would be solely on the surface of the NW. Such an observation opens up the possibility of using photocurrent behavior in oxygen sensing rather than monitoring dark current. Oxygen sensing is an important issue in many fields, such as the environment, medicine, transportation,

[1]Department of Electrical Engineering and Institute of Microelectronics, Center for Micro/Nano Science and Technology Advanced Optoelectronic Technology Center, National Cheng Kung University, Tainan, Taiwan; [2]Institute of Atomic and Molecular Sciences, Academia Sinica, Taipei, Taiwan; [3]Institute of Biophotonics, National Yang-Ming University, Taipei, Taiwan; [4]Biophotonics and Molecular Imaging Research Centre, National Yang-Ming University, Taipei, Taiwan; [5]Graduate Institute of Applied Science and Technology, National Taiwan University of Science and Technology Taipei, Taiwan and [6]Center for Condensed Matter Sciences, National Taiwan University, Taipei, Taiwan
Correspondence: Professor K-H Chen, Institute of Atomic and Molecular Sciences, Academia Sinica, No. 1, Sector 4, Roosevelt Road, Taipei 106, Taiwan.
E-mail: chenkh@pub.iams.sinica.edu.tw
Received 12 December 2012; revised 7 February 2013; accepted 12 February 2013

meteorology and agriculture. For example, oxygen sensors can monitor the environmental oxygen concentration of an industrial clean room; they are also widely used to control the air/fuel ratio in automobile engines, which enhances combustion efficiency and reduces the emission of pollutants. In this study, we report a photo-enhanced (visible light) transport modulation approach for sensing molecular oxygen by applying a low bias at room temperature to a single Au-NPs@silica NW device. A model for the electrical transport properties and the sensing mechanism is discussed.

EXPERIMENTAL PROCEDURE

The Au-NPs@silica NWs were synthesized by microwave plasma-enhanced chemical vapor deposition) using a microreactor technique.[14] Briefly, the microreactor is a sandwich configuration substrate for guiding a flowing stream of precursor gas. A gold-coated (28–112 nm) Si wafer was placed on top of a Au (7 nm)/SiN_x (200 nm)-coated Si substrate in a sandwich configuration, which was placed into the reaction chamber for synthesis. The morphologies of the single Au-NPs@silica NWs were characterized using field-emission scanning electron microscopy (JEOL 6700F; JEOL Ltd., Tokyo, Japan). The crystallographic and structural properties of the NWs were characterized using a Philips FEI TECNAI G^2 high-resolution TEM operated at 200 kV (Gatan Inc, Pleasanton, CA, USA). For electrical measurements, the NWs were supported on an ~200-nm silicon dioxide (SiO_2)-coated commercial silicon (100) wafers. Individual NW devices were fabricated using electron-beam nanolithography and lift-off techniques. The electrical characteristics of the single NW devices were measured in an ultralow leakage current ($\sim 1 \times 10^{-14}$A) probe station at room temperature under vacuum. A semiconductor characterization system (Keithley model 4200-SCS, Keithley Instrument, Inc., Cleveland, OH, USA) was utilized to apply dc bias and measure the current. All photoresponse and sensing measurements were performed with a 1-V dc bias. A 532-nm diode laser with a power of 5 mW was used as the excitation source in the photocurrent measurements. The purity of the air used was similar to that of ambient air with a relative humidity ~40%, and the purity of the oxygen used was ~99.995%.

RESULTS AND DISCUSSION

A field-emission scanning electron microscopy image of the microwave plasma-enhanced chemical vapor deposition-grown ensemble Au-NPs@silica NWs is displayed in Figure 1a. The lengths and diameters of the NWs were in the ranges of 1–3 μm and 50–80 nm, respectively. Figure 1b shows a TEM image of one randomly selected Au-NPs@silica NW. The Au NP size and inter-distances were ~30 nm and ~200 nm, respectively. A typical high-resolution TEM image (Figure 1c) confirms that the crystal structure of the Au core is single crystalline, whereas the silica NW itself is amorphous.

Figures 2a and b show field-emission scanning electron microscopy images of two terminal single-NW devices consisting of a silica NW without Au NPs and a Au-NPs@silica NW, respectively. To understand the basic electrical and optoelectronic properties of the single-NW devices, the conventional current–voltage (*I–V*) and photoresponse were measured at room temperature in vacuum. As shown in Figure 2c, the *I–V* plots of both NWs are linear, indicating the ohmic nature of the *e*-beam defined contacts. The slope of the *I–V* plot indicates that the electrical conductivity of the Au-NPs@silica NW is higher than that of the bare silica NW. This trend occurs, because the creation of more electron-hopping sites in the Au-NPs@silica NW leads to enhanced conductivity, as we have reported previously.[18] During the growth of Au NP-peapodded silica NWs, residual Au atoms may partially incorporate into the silica matrix of the wire during peapod formation.[14] The incorporation of Au could produce impurities and/or defect-related hopping sites in the silica matrix.[18] The Au-embedded silica NW has higher conductivity than the plain silica NW, because of its shorter hopping length. Photoresponse measurements of the NW devices were conducted under alternating 532-nm illumination and dark conditions, as shown in Figure 2d. The plain silica NW device does not show any significant photoresponse; the ratio of photo and dark current is ~0.01. In contrast, the Au-NPs@silica NW device presents a reversible photoresponse and a stable photocurrent, with a photo/dark current ratio of ~1.48. Assuming the band gap of silica NWs to be in the range of ~6.8 eV[15] and denying any absorption of the 532-nm light, these data suggest that the photocurrent can be attributed to the near-resonance SP absorption of the Au NPs (within the silica NWs) that has been reported at ~532 nm.[14] The SPR-dominant photoconduction can be further confirmed by the photoresponsivity spectrum of a single Au-NPs@silica NW (see Supplementary Figure S1).

Furthermore, to understand the observed enhanced photocurrent behavior, we analyzed the electric-field profiles and the associated optical characteristics using finite difference time domain simulation methods. The simulation of the NW structure was performed using its experimental geometry and the standard values of the refractive index of Au and SiO_2 from the literature. Figure 3 shows the

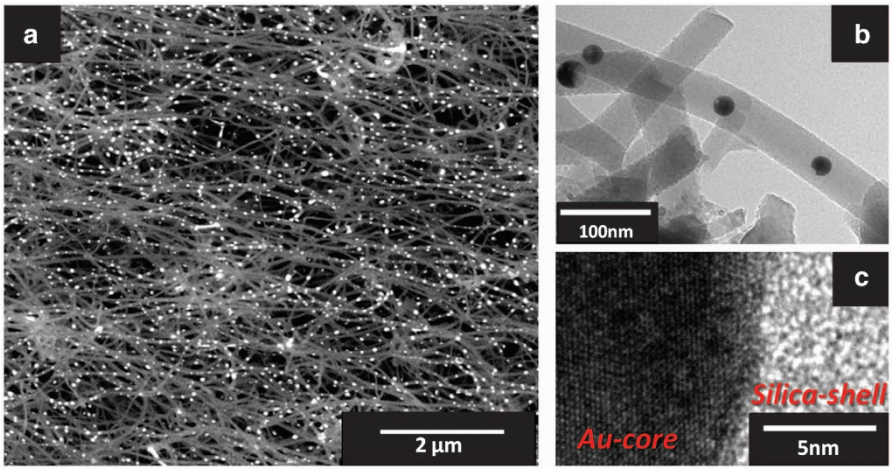

Figure 1 (**a**) Field-emission scanning electron microscopy image at low magnification and (**b**) TEM image at high magnification of the Au-peapodded silica NWs that were synthesized with a microwave plasma-enhanced chemical vapor deposition system, showing the silica sheath and Au NPs within. (**c**) High-resolution TEM image of a single Au-NPs@silica NW, showing the metallic core and an amorphous sheath.

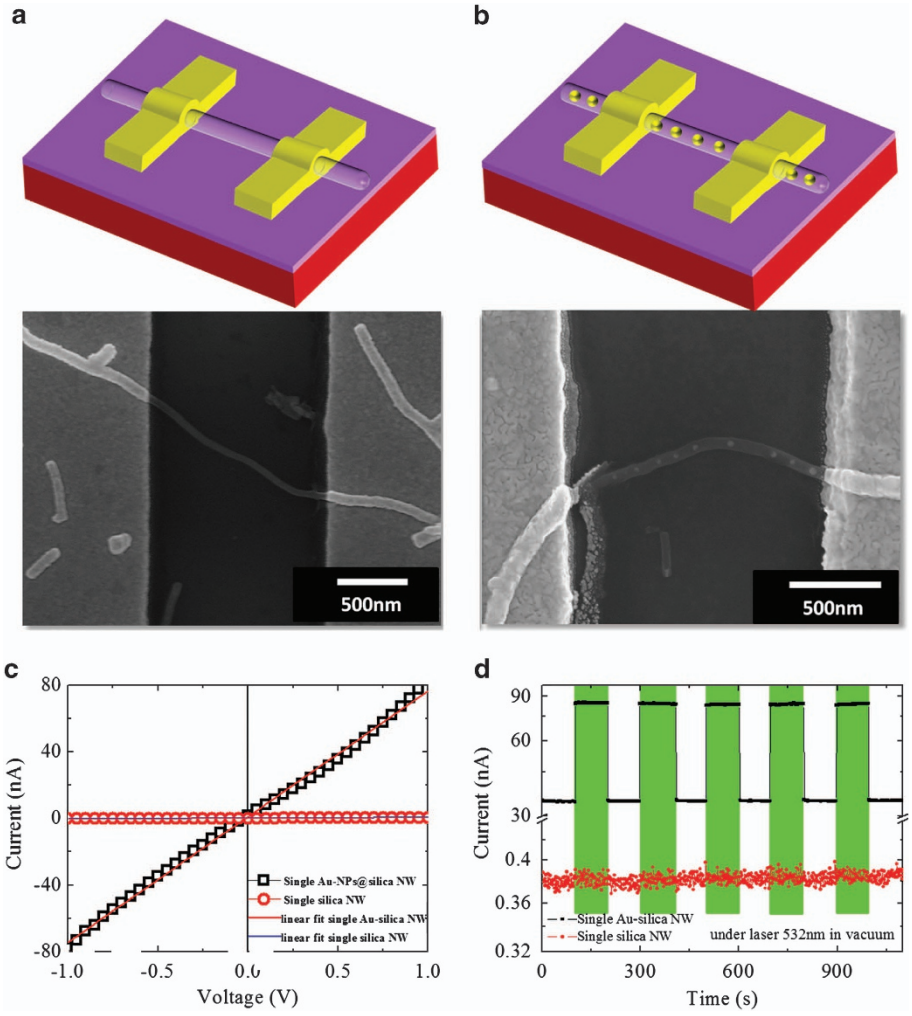

Figure 2 Field-emission scanning electron microscopy images of single NW devices consisting of (**a**) plain silica NW (without the Au NPs) and (**b**) Au-NPs@silica NW. (**c**) Dark *I–V* characteristics of single NW devices, with and without the Au NP peapods, measured in vacuum, and the corresponding linear fit to the data set. (**d**) Dark and photocurrent measured under vacuum in single NW devices, with and without the Au NP peapods, as a function of time. The colored bars indicate the duration of the 532-nm illumination. The measurement was performed with a 1-V applied bias at room temperature. The bare silica NW showed no photoresponse, whereas the Au-NP@Silica NW showed strong photoresponse.

electric-field intensity distributions of plain SiO_2 NWs (Figure 3a) and Au-NPs@SiO_2 NWs (Figure 3b) under an incident wavelength of 532-nm polarized light transverse to the NW (transverse electric (E⊥NW) and transverse magnetic (E//NW)). The finite difference time domain simulation results indicate that the plain SiO_2 NW did not show any unique SPR absorption under 532-nm wavelength excitation for both transverse electric and transverse magnetic modes, as shown in Figure 3a. In contrast, the electric-field profile of the Au-NPs@SiO_2 NW (Figure 3b) for both transverse electric and transverse magnetic modes under 532-nm excitation displays a significantly stronger localized SPR-enhanced electric field at the Au NP surface than the plain silica NW. These simulated electric-field profiles are in good agreement with the enhanced photocurrent response (Figure 2d) and absorption spectrum[14] of the Au-NPs@silica NWs.

To realize the sensitivity of the Au-NPs@silica NW device to oxygen, it is critical to understand its properties in a regular atmosphere containing roughly (by volume) 78.08% nitrogen (N_2), 20.95% oxygen (O_2) and 0.93% argon (Ar).[19]

The real-time current response of the individual Au-NPs@silica NW device was measured in air and a pure N_2 environment under various pressures at room temperature. As shown in Figure 4, the Au-NPs@silica NW devices do not show any significant current variation in the N_2 atmosphere, irrespective of the pressure range studied. However, when measured in air, the current in the Au-NPs@silica NWs decreased monotonically with the increase in air pressure. This result implies that the Au-NPs@silica NWs have good selectivity for O_2 molecules in air (neglecting the effect of trace gases). Desorbing all the adsorbed O_2 molecules from the NW surface and recovering the original current level by pumping down to $\sim 5 \times 10^{-4}$ Torr were difficult. However, gentle heating of the device from 300 to 350 K could remove the remaining adsorbed molecules from the NW surface and restore the original current value at 300 K (see Supplementary Figure S2).

The conductance of a single Au-NPs@silica NW can be calculated by[20,21]

$$G = n_o e \mu \pi R^2 / L \quad (1)$$

where n_o is the original carrier concentration, e is the electronic charge, μ is the electronic mobility, and R and L are the radius and length of the NW between the electrodes, respectively.

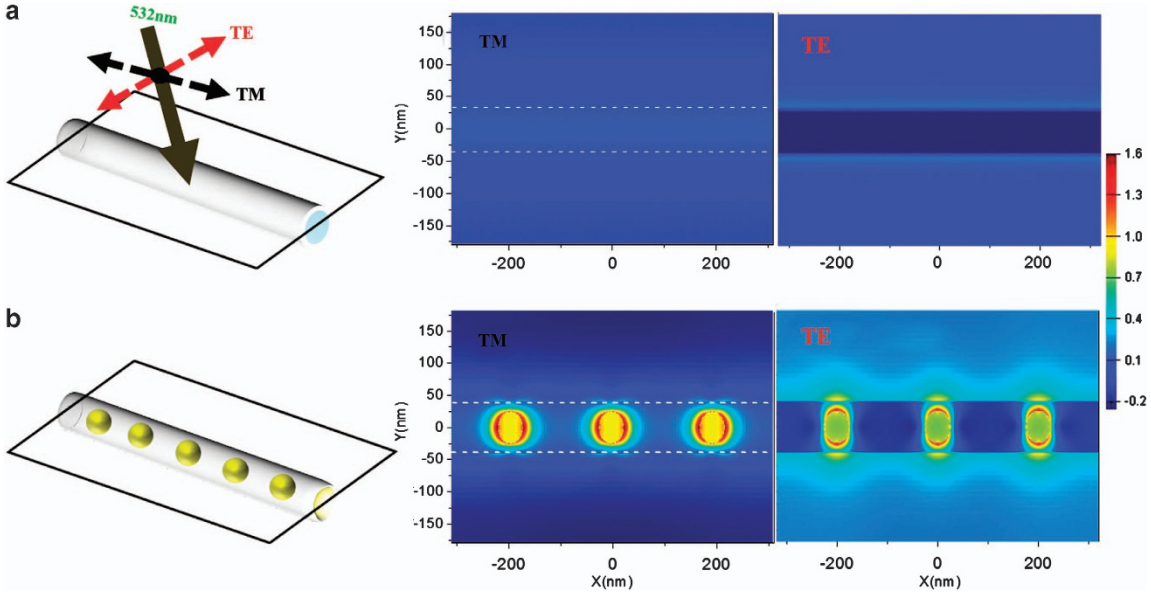

Figure 3 The finite difference time domain simulation of electric-field intensity for (**a**) plain SiO_2 NWs and (**b**) Au-NPs@SiO_2 NWs.

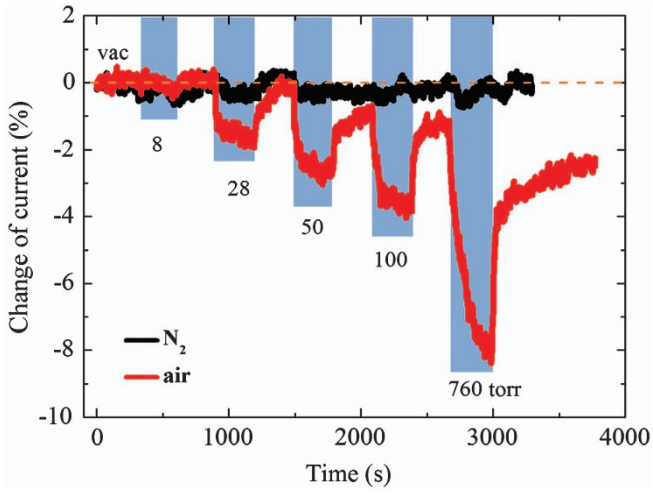

Figure 4 Dark-current dynamics observed in the single AuNP@silica NW device when exposed to pure nitrogen and air. The colored bars indicate the time duration for which the gases were flown into the measuring chamber. The dark current shows strong selectivity for air (containing oxygen) rather than nitrogen.

During gas sensing, the target gas will be adsorbed on the NW surface, changing its conductance, which is attributed to the changes in surface-carrier concentrations ($^{\Delta}n_s$), because all other factors in equation (1) are either constants or assumed invariant under the experimental conditions. This change can be described by the equation

$$\Delta G = \Delta n_s e \mu \pi R^2 / L \tag{2}$$

Hence, the gas response of the device is given by the following:

$$\frac{\Delta G}{G} = \frac{\Delta n_s}{n_o} \tag{3}$$

Equation (3) suggests that a large change in the carrier concentration could increase the sensitivity of the measurement. This conjecture can be verified by illuminating our Au-NPs@silica NW system to increase the carrier concentration and then testing the sensing performance.

Figures 5a and b show schematic diagrams of the single plain silica NW and the single Au-NPs@silica NW devices, respectively, illuminated with 532-nm wavelength light for the gas-sensing measurements. The normalized photoresponse of the Au-NPs@silica NW device was measured in vacuum and under various O_2 pressures under illumination with 532-nm light (Figure 5c). In contrast, the plain silica NW device does not show any photoresponse under similar variations of O_2 pressure (Figure 5d). The photocurrent of the Au-NPs@silica NW, however, decreased with increasing O_2 pressure. To determine the O_2-sensing ability under dark and illuminating (532-nm excitation) conditions, we define the response as

$$Response = \frac{I_{vac} - I_{O_2}}{A_{NW}} \tag{4}$$

where A_{NW} is the NW surface area, and I_{vac} and I_{O_2} are the current levels in a vacuum and O_2 environment, respectively. Figures 5e and f show the variation in the response (equation 4) of the plain silica NW and the Au-NPs@silica NW under both photo and dark conditions, under various O_2 pressures. The response of the plain silica NW does not show any apparent variation under dark or illuminated conditions (Figure 5e). In contrast, the response of the Au-NPs@silica NW was enhanced approximately twofold under illumination with 532-nm light.

For practical applications, in addition to response, the recovery time (time to attain initial current value from saturation value under the given O_2 pressure) is also an important parameter. The current in the Au-NPs@silica NW was investigated at an oxygen pressure of 500 Torr, under both dark conditions and 532-nm light (Figures 6a and b) as a function of time. The current recovery time of the Au@NPs silica NW device under illumination was 750 s faster than that under dark conditions (Figure 6b). Thus, the Au-NPs@silica NW device is demonstrably a better sensing device under illumination than under dark conditions.

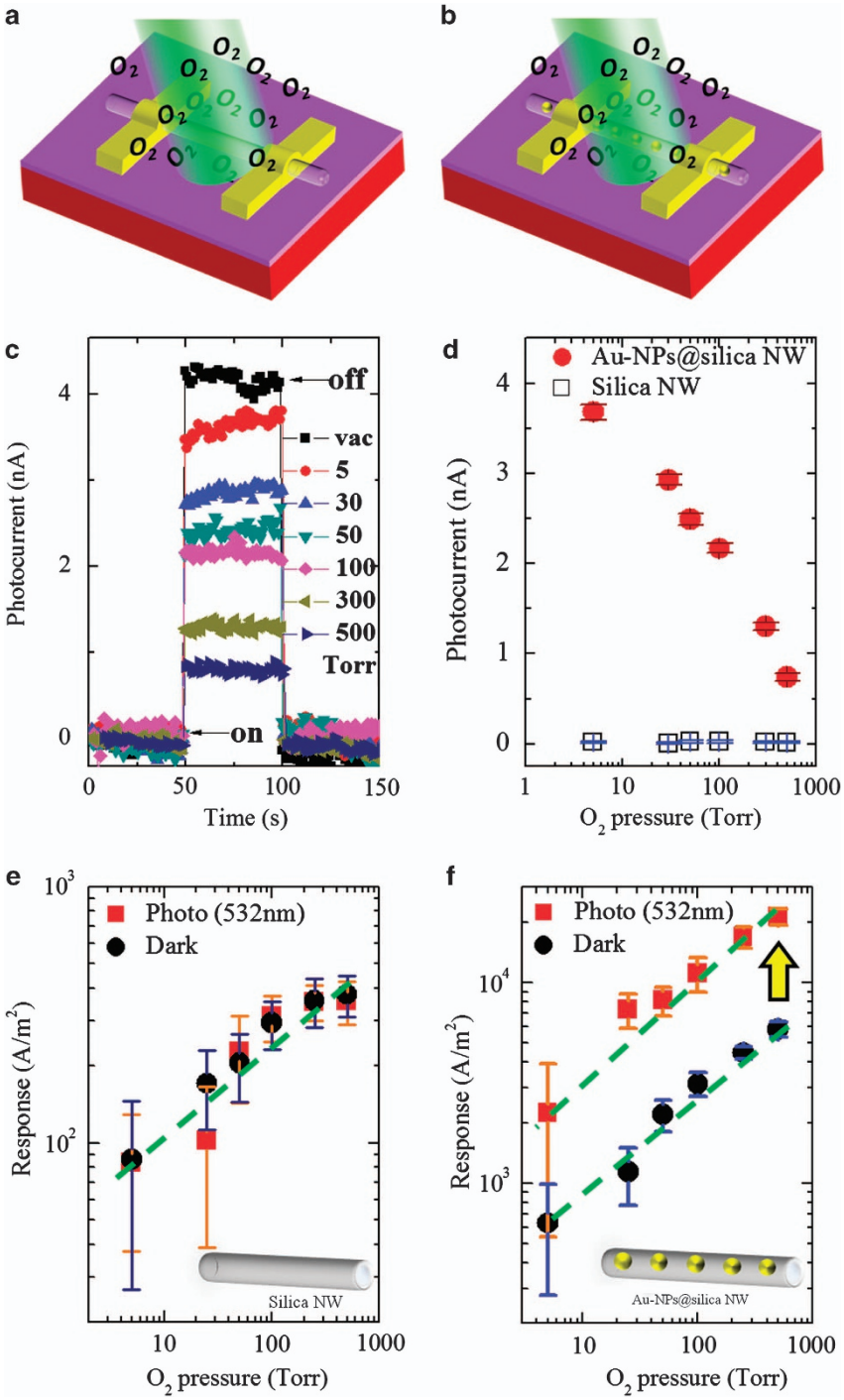

Figure 5 Sketches showing the single plain silica NW (**a**) and single Au-NPs@silica NW (**b**) devices under illumination for gas sensing. (**c**) Photocurrent dynamics, as a function of time, of the single Au-NP@silica NW device under various oxygen pressures. (**d**) Photocurrent as a function of oxygen pressure in single silica NW devices with and without the Au NPs. The O_2-sensing responses as a function of oxygen pressure for (**e**) the plain silica NW and (**f**) the Au-NPs@silica NW under photo (532 nm) and dark conditions.

Lastly, the details of the photo-enhanced oxygen-sensing mechanism, shown in a schematic (Figure 7) for the Au-NPs@silica NW device, has to be described to complete this report. The Au-NPs@silica NW is a nonstoichiometric silica matrix[14] with an Si/O atomic ratio of 1:0.6, obtained on the NW shell by TEM energy dispersive spectrometer (EDX) analysis, which implies an inherent affinity of the surface for oxygen molecules. Under dark conditions, the O_2 molecules adsorbed at the NW surface capture available free electrons, leading to the reduction of conductance (G) following the reaction:[22]

$$O_2(g) + e^- \rightarrow O_2^-(ad) \quad (5)$$

We assumed that the surface-defect concentrations of both Au-NPs@silica NW and plain silica NWs were equal, due to the

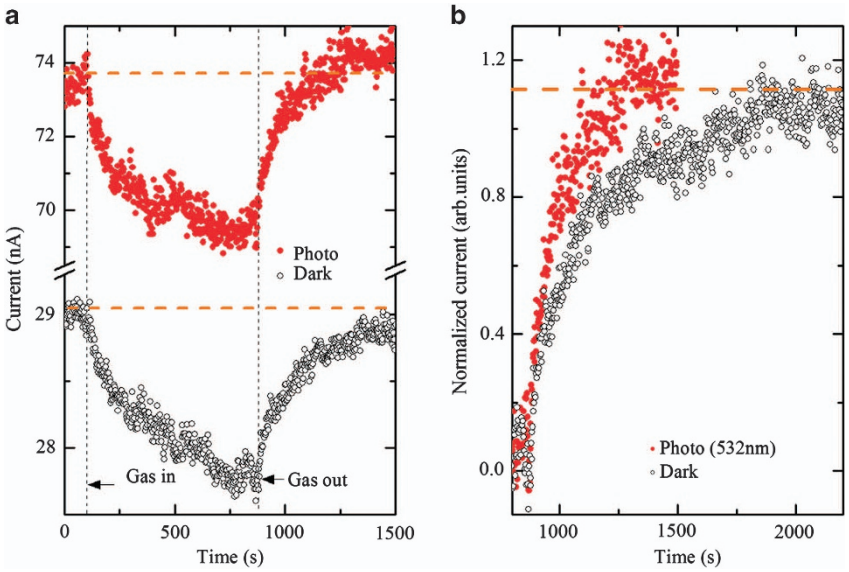

Figure 6 (**a**) Current dynamics in the single Au-NP@silica NW device under illuminating and dark conditions with an oxygen pressure of 500 Torr. (**b**) Photo and dark current, normalized with respect to the initial current value in vacuum, as a function of time in Au-NPs@silica NWs (at an oxygen pressure of 500 Torr), showing faster recovery of the current under illuminating conditions. All measurements are performed with a 1V bias and at room temperature.

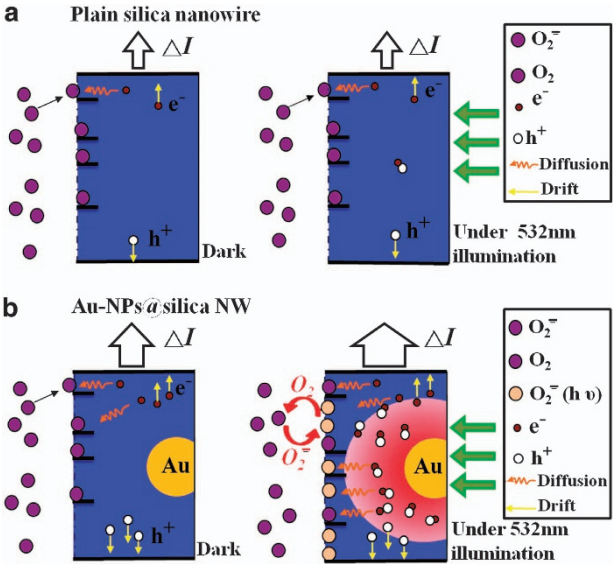

Figure 7 Electron transport mechanisms for the (**a**) plain silica NW and (**b**) Au-NPs@silica NW under dark and illuminating conditions, respectively. Surface defects control the conductivity of the plain silica NW in **a**, with no photoresponse due to the wide band gap. The conductivity of the Au-NP@silica NW (**b**) is controlled by both the surface states and carriers contributed by the Au NPs. Under 532-nm excitation, SP absorption creates excess carriers that contribute to the higher conductivity.

identical growth process used for both. However, the Au-NPs@silica NW has a higher density of electron-hopping sites than the plain silica NW; the charge carriers use these sites for transport through the NW during the sensing event and finally when collected by the electrodes.[18] Therefore, the high effective conductivity of the Au-NPs@silica NWs surrounding the chemisorbed oxygen molecules was crucial for the gas sensor to enhance the sensing response. However, the number of surface-defect sites in the single NW available for the adsorption of oxygen molecules is finite, which limits the sensitivity and response of the NW (Figures 7a and b) under high O_2 pressures.

Pao *et al.*[15] studied the SP intensity profiles of Au-NPs@silica NWs with three selected energies, filtered to 1.65–2.15 eV (red), 2.05–2.55 eV (green) and 2.85–3.35 eV (blue) by the field-emission TEM system. The results revealed that the largest SP intensity is achieved under green illumination, compared with red and blue illumination, because of the SPR effect. Thus, under SPR wavelength (532-nm, green) photo-excitation, the photo-electrons in the Au NPs peapod can move across the Au NPs/silica NW interface into unoccupied localized or defect hopping sites in the silica NW and transport across the silica NW via hopping.

The photo-enhanced gas-sensing mechanism is a three-step process. The first step is optical absorption, which is determined by the optical-electrical energy conversion efficiency, that is, quantum efficiency. The second and third steps are charge-hopping transport and interactions between the mobile charge and gas molecules. The Au NPs are actually involved in the first step, that is, optical absorption or quantum efficiency via enhanced SPR absorption. After that step, charge transport will follow the hopping transport process.

Thus, under 532-nm excitation conditions, the SPR effect induces photocurrent within the Au-NP@silica NW,[14] which contributed more carriers to improve the sensing response (larger current). The photo-induced holes migrate to the NW surface due to the field at the semiconductor-air interface[23] and discharge the chemisorbed oxygen ions following the reaction

$$h^+(h\upsilon) + O_2^-(ad) \rightarrow O_2(g) \quad (6)$$

Simultaneously, the photo-induced electrons will react with O_2 gas molecules to form photo-activated oxygen ions (O_2^- hν) adsorbed on the silica NW surface following this reaction equation[24]

$$O_2(g) + e^-(h\upsilon) \rightarrow O_2^-(h\upsilon) \quad (7)$$

These processes compete to achieve an equilibrium for which a saturated current value was obtained. To our understanding, the electron is more associated with the oxygen 'adsorption' reaction.

The hot electron is created by the resonance of SPs when the frequency of light couples with the SP frequency of the Au NPs. For the plain silica NW, illumination did not cause any change in current or response, because the 532-nm excitation was much lower than the 6.8-eV band gap.[15]

In the Au-NPs@silica NW, the effective oxygen adsorption includes adsorptions at the surface states and those activated by photo-electrons ($O_2^- h\nu$), which increases the response of various oxygen pressures under illumination. For the recovery (desorption) process, the ambient atmosphere changes from O_2 to vacuum, and the photogenerated holes react with the oxygen ions on the surface, releasing them in the form of oxygen gas, following equation 6. The recovery time for oxygen sensing (Figure 6b) is determined by the oxygen desorption rate from the NW. Under illumination, the photogenerated hole could increase the oxygen desorption rate and recovery time by the reaction (equation 6). This effect would make the oxygen recovery time faster under photo-excitation than under dark conditions, as no holes participate in the oxygen desorption reaction in the dark. SPR-induced visible light absorption in Au-NPs@silica NW provides improved oxygen selectivity, response and recovery time.

CONCLUSIONS

In conclusion, a method of photo-assisted (532 nm) oxygen gas sensing with individual Au-NPs@silica NWs is demonstrated vis-à-vis systems and those using plain silica NW at room temperature. The Au-NPs@silica NW produces an oxygen pressure-dependent photocurrent that is stable and reversible upon removal of oxygen. The superior sensing response originates from SP-induced absorption in the Au NPs and the production of photogenerated electrons and holes that was prohibited in plain silica NW, which has a wide band gap. The photogenerated holes help in the removal of surface oxygen and, hence, recovery of the pristine surface to start a fresh sensing cycle. The recovery time is appreciably faster than that of plain silica NWs. A schematic mechanism for sensing in these single NW devices is proposed.

ACKNOWLEDGEMENTS

This work was supported by the Ministry of Education, National Science Council, National Taiwan University, National Cheng Kung University (NCKU), National Yang-Ming University and Academia Sinica, Taiwan. Technical support was provided by the Core Facilities for Nano Science and Technology, Academia Sinica and National Taiwan University. Fruitful discussion and technical help from Dr Han Hsieh-Cheng was also appreciated.

1 Banan, Sadeghian, R. & Islam, M. S. Ultralow-voltage field-ionization discharge on whiskered silicon nanowires for gas-sensing applications. *Nat. Mater.* **10,** 135–140 (2011).
2 Wang, S. -B., Hsiao, C. -H., Chang, S. -J., Lam, K. -T., Wen, K. -H., Young, S. -J., Hung, S. -C. & Huang, B. -R. CuO nanowire-based humidity sensor. *IEEE Sens. J.* **12,** 1884 (2012).
3 Chen, R. -S., Wang, S. -W., Lan, Z. -H., Tsai, J. T. -H., Wu, C. -T., Chen, L. -C., Chen, K. -H., Huang, Y. -S. & Chen, C. -C. On-chip fabrication of well-aligned and contact-barrier-free GaN nanobridge devices with ultrahigh photocurrent responsivity. *Small* **4,** 925–929 (2008).
4 Liu, S. & Guo, X. Carbon nanomaterials field-effect-transistor-based biosensors. *NPG Asia Mater.* **4,** 1–10 (2012).
5 Jana, D., Chen, L. -C., Chun-Wei, C., Chattopadhyay, S. & Chen, K. -H. A first principles study of the optical properties of BxCy single wall nanotubes. *Carbon NY* **45,** 1482–1491 (2007).
6 Lin, Y. -G., Hsu, Y. -K., Chen, S. -Y., Chen, L. -C. & Chen, K. -H. Microwave-activated CuO nanotip/ZnO nanorod nanoarchitectures for efficient hydrogen production. *J. Mater. Chem.* **21,** 324–326 (2011).
7 Burda, C., Chen, X., Narayanan, R. & El-Sayed, M. A. Chemistry and properties of nanocrystals of different shapes. *Chem. Rev.* **105,** 1025–1102 (2005).
8 Law, J. B. K. & Thong, J. T. L. Improving the NH3 gas sensitivity of ZnO nanowire sensors by reducing the carrier concentration. *Nanotechnology* **19,** 205502 (2008).
9 Russell, D. M., Newsome, C. J., Li, S. P., Kugler, T., Ishida, M. & Shimoda, T. Blends of semiconductor polymer and small molecular crystals for improved-performance thin-film transistors. *Appl. Phys. Lett.* **87,** 222109 (2005).
10 Kolmakov, A., Klenov, D. O., Lilach, Y., Stemmer, S. & Moskovits, M. Enhanced gas sensing by individual SnO2 nanowires and nanobelts functionalized with Pd catalyst particles. *Nano Lett.* **5,** 667–673 (2005).
11 Zhang, Y., Kolmakov, A., Lilach, Y. & Moskovits, M. Electronic control of chemistry and catalysis at the surface of an individual tin oxide nanowire. *J. Phys. Chem. B* **109,** 1923–1929 (2005).
12 Wan, Q., Huang, J., Xie, Z., Wang, T., Dattoli, E. N. & Lu, W. Branched SnO2 nanowires on metallic nanowire backbones for ethanol sensors application. *Appl. Phys. Lett.* **92,** 102101 (2008).
13 Luo, L., Sosnowchik, B. D. & Lin, L. Local vapor transport synthesis of zinc oxide nanowires for ultraviolet-enhanced gas sensing. *Nanotechnology* **21,** 495502 (2010).
14 Hu, M. S., Chen, H. L., Shen, C. H., Hong, L. S., Huang, B. R., Chen, K. H. & Chen, L. C. Photosensitive gold-nanoparticle-embedded dielectric nanowires. *Nat. Mater.* **5,** 102–106 (2006).
15 Pao, C. -W., Wu, C. -T., Tsai, H. -M., Liu, Y.- S., Chang, C. -L., Pong, W. F., Chiou, J. -W., Chen, C. -W., Hu, M. -S., Chu, M. -W., Chen, L. -C., Chen, C. -H., Chen, K. -H., Wang, S. -B., Chang, S. -J., Tsai, M. -H., Lin, H. -J., Lee, J. -F. & Guo, J. -H. Photoconduction and the electronic structure of silica nanowires embedded with gold nanoparticles. *Phys. Rev. B* **84,** 165412 (2011).
16 Hsieh, C. H., Chou, L. J., Lin, G. R., Bando, Y. & Golberg., D. Nanophotonic switch: gold-in-Ga2O3 peapod nanowires. *Nano Lett.* **8,** 3081–3085 (2008).
17 Wu, C. -T., Chu, M. -W., Wang, S. -B., Hu, M. -S., Chen, K. -H., Chen, L. -C., Chen, C. -W. & Chen, C. -H. Anisotropic surface plasmon excitation in Au/silica nanowire. *Appl. Phys. Lett.* **96,** 263106 (2010).
18 Wang, S. -B., Hu, M. -S., Chang, S. J., Chong, C. -W., Han, H. -C., Huang, B. -R., Chen, L. -C. & Chen, K. -H. Gold nanoparticle-modulated conductivity in gold peapodded silica nanowires. *Nanoscale* **4,** 3660–3664 (2012).
19 Zhang, J., Lu, Z. H. & Wang, L. J. Precision refractive index measurements of air, N-2, O-2, Ar, and CO2 with a frequency comb. *Appl. Optics* **47,** 3143–3151 (2008).
20 Fan, Z. & Lua, J. G. Gate-refreshable nanowire chemical sensors. *Appl. Phys. Lett.* **86,** 123510 (2005).
21 Ramgir, N. S., Yang, Y. & Zacharias, M. Nanowire-based sensors. *Small* **6,** 1705–1722 (2010).
22 Kind, H., Yan, H. Q., Messer, B., Law, M. & Yang, P. Nanowire ultraviolet photodetectors and optical switches. *Adv. Mater.* **14,** 158–160 (2002).
23 Winer, K. Band bending and oxygen-induced defects in a-Si-H. *J. Vac. Sci. Technol. B* **7,** 1226–1231 (1989).
24 Fan, S. -W., Srivastava, A. K. & Dravidc, V. P. UV-activated room-temperature gas sensing mechanism of polycrystalline ZnO. *Appl. Phys. Lett.* **95,** 142106 (2009).

Supplementary Information accompanies the paper on the NPG Asia Materials website (http://www.nature.com/am)